Modeling the Multiphase Flow in a Dense Medium Cyclone

ARTICLE *in* INDUSTRIAL & ENGINEERING CHEMISTRY RESEARCH · APRIL 2009

Impact Factor: 2.59 · DOI: 10.1021/ie801175c

Modeling the Multiphase Flow in a Dense Medium Cyclone

B. Wang,[†] K. W. Chu,[†] A. B. Yu,*[,†] and A. Vince[‡]

Laboratory for Simulation and Modelling of Particulate Systems, School of Materials Science and Engineering, The University of New South Wales, Sydney, NSW 2052, Australia, and Elsa Consulting Group Pty Ltd., Mackay, Qld 4740, Australia

A mathematical model is proposed to describe the multiphase flow in a dense-medium cyclone (DMC). In this model, the volume of fluid multiphase model is first used to determine the shape and position of the air core, and then the mixture multiphase model is employed to describe the flow of the dense medium (comprising finely ground magnetite in water) and the air core, where the turbulence is described by the Reynolds stress model. The results of fluid flow are finally used in the simulation of coal particle flow described by the stochastic Lagrangian particle tracking model. The validity of the proposed approach is verified by the reasonably good agreement between the measured and predicted results under different conditions. The flow features in a DMC are then examined in terms of factors such as flow field, pressure drop, particle trajectories, and separation efficiency. The results are used to explain the key characteristics of flow in DMCs, such as the origin of a short-circuit flow, the flow pattern, and the motion of coal particles. Moreover, the so-called surging phenomenon is examined in relation to the instability of fluid flow. The model offers a convenient method to investigate the effects of variables related to geometrical and operational conditions on the performance of DMCs.

1. Introduction

Dense-medium cyclones (DMCs), also known as heavy-medium cyclones, are the work horses of the modern coal industry to upgrade run-of-mine coal in the 0.5−50 mm size range. Its working principle has been well documented.[1−3] Since its invention about 50 years ago (followed by continuous innovative modifications), DMCs have been proved to be effective in coal industry. Today, DMCs process the vast majority of tonnes fed to coal preparation plants.

The flow in a DMC is very complicated with the presence of swirling turbulence, air core, and segregation, and involves multiphases: gas, liquid, coal, and magnetic/nonmagnetic particles of different sizes and densities. Normally, the slurry including water, magnetite, and nonmagnetic particles is named "medium" in practice. Precise measurement of the velocity field in a DMC is very difficult, mainly because of the presence of magnetite particles in the medium. However, in the past decade or so, significant experimental research has been carried out with hydrocyclones where dense medium is absent and where the measurements are relatively easy to make.[2,4−11] For example, Hsieh et al.[7,8] reported a comprehensive experimental study of the fluid flow pattern, pressure drop, and solids motion in a 75 mm hydrocyclone using laser doppler velocimetry (LDV). From these results, the flow field in a hydrocyclone was deduced. However, data of a similar degree of detail are not available for DMCs, with available results being limited to the effects of geometrical and operational conditions on DMC performance.[12−20] The density distribution of medium in a DMC has been reported by Galvin and Smitham[21] using X-ray tomography and by Subramanian[22] using gamma ray tomography (GRT).

Designers/controllers rely traditionally on empirical equations for predicting the equipment performance as a function of variables related to operational, geometrical, and materials conditions, and in the past many studies have been made in this direction.[12,13,15,17−19,23−31] Different sets of experimental data lead to different equations even for the same basic parameters. Current understanding of how a DMC operates is largely based on the ground-breaking work undertaken over 25 years ago based on 750 mm and smaller units. Recent research efforts have been extended to larger and more modern units, mainly by correlation analysis of the results from the difficult and costly pilot-scale experiments.[32−37] However, this would not lead to much improved understanding of the underlying fundamentals under different conditions, and the outcomes often have limited applicability. For example, such an empirical equation can only be used within the extremes of the experimental data from which the model parameters were determined. Therefore, development of a computer model that can describe the fundamentals governing the multiphase flow and predict the performance of DMC under different production conditions has been recognized as an important step to overcome this problem.

In the past two decades or so, various efforts have been made to develop such a mathematical model based on the flow fundamentals and computational fluid dynamics (CFD). One of the earliest numerical models was due to Zughbi et al.[31] This was an oversimplified approach in which axis symmetry was assumed and the Prandtl mixing-length turbulence model adopted. Suasnabar and Fletcher[38] reported a 2D model to predict the velocity distribution in a 200 mm DMC. Brennan[39] used a mixture multiphase flow model to simulate the medium segregation under the experimental conditions of Subramanian.[22] The model was further developed by Narasimha et al.,[40] which could satisfactorily describe the density distribution in a 350 mm DMC, but somehow the predicted velocity profile in the inner flow and air core did not follow the normal understanding in hydrocyclones.

This Article reports our recent effort in modeling the gas−liquid−solid flow in a DMC. It shows that the combination of the Reynolds stress model (RSM), volume of fluid (VOF) free surface model, mixture model, and stochastic Lagrangian model can satisfactorily describe the flow and performance of

* To whom correspondence should be addressed. Fax: + 61 2 93855956. E-mail: a.yu@unsw.edu.au.
[†] The University of New South Wales.
[‡] Elsa Consulting Group Pty Ltd.

10.1021/ie801175c CCC: $40.75
Published on Web 02/13/2009

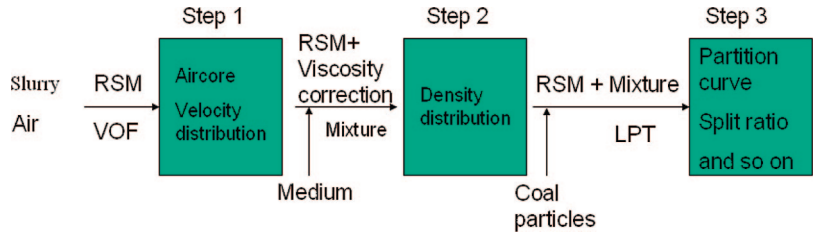

Figure 1. Steps used in the present modeling.

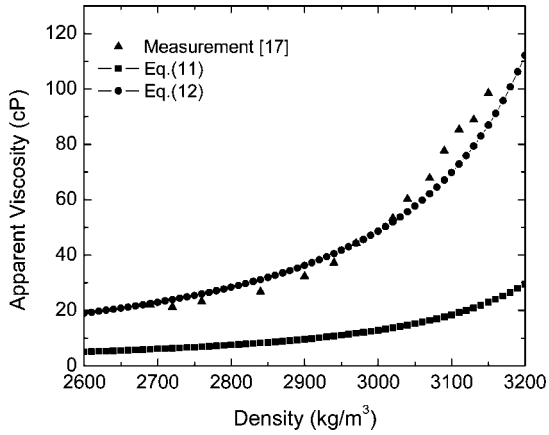

Figure 2. The relationship between the medium viscosity and the fluid density.

a DMC. The model should be useful in assessing the performance of DMCs under different production conditions.

2. Model Description

2.1. Model Strategy. Recognizing that the flow in a DMC is quite complicated, the modeling was divided into three steps as shown in Figure 1. In step 1, only air and slurry with a certain density are considered. The two phases are treated as a fluid of homogeneous viscosity and density. Its flow turbulence is modeled using the RSM, and the VOF free surface model is used to describe the interface between the medium (defined as the mixture of water and magnetite) and the air core (here defined as the region with volume fraction of air larger than 90%). In this step, the primary position of air core and the initial velocity distribution are obtained. They are used as part of the initial conditions for the next step to speed up the computation. The method is similar to that used for modeling the multiphase flow in a hydrocyclone.[41]

In step 2, six additional phases are introduced to describe the behavior of magnetite particles with different sizes. The multiphase model is changed from the VOF to the so-called mixture multiphase model.[42] A correction is also necessary to estimate the viscosity effect of the magnetite particle size distribution. Detailed density and velocity distributions of different phases are obtained at the end of this step.

In step 3, the results of the fluid flow are used in the simulation of the flow of coal particles described by the stochastic Lagrangian particle tracking model (LPT). The characteristics of the DMC separating performance, such as partition coefficient curve and medium split, are then estimated.

Therefore, the whole process involves four CFD models for different phases and one viscosity correction model, as described below.

2.2. Governing Equations for Medium Flow and Turbulence Model. For the incompressible fluid flow in a cyclone, the equations of continuity and momentum, named the Reynolds-averaged Navier−Stokes equations (RANS), can be expressed as[43]

$$\frac{\partial \rho}{\partial t} + \frac{\partial}{\partial x_i}(\rho u_i) = 0 \tag{1}$$

$$\frac{\partial}{\partial t}(\rho u_i) + \frac{\partial}{\partial x_j}(\rho u_i u_j) = -\frac{\partial p}{\partial x_i} + \frac{\partial}{\partial x_j}\left[\mu\left(\frac{\partial u_i}{\partial x_j} + \frac{\partial u_j}{\partial x_i}\right)\right] + \frac{\partial}{\partial x_j}(-\rho\overline{u_i' u_j'}) \tag{2}$$

where the velocity components are decomposed into the mean $\bar{u}_i$ and fluctuating u'_i velocities ($i = 1, 2, 3$). They are related, as given by

$$u_i = \overline{u_i} + u_i' \tag{3}$$

where the Reynolds stress term $-\rho\overline{u'_i u'_j}$ includes the turbulence closure, which must be modeled to close eq 2.

The turbulence model is based on the transport equations for all components of the Reynolds stress term and the respective dissipation rate. RSM can describe this anisotropic turbulence flow. At this stage of development, it is in fact considered the most appropriate turbulence model for cyclone flow, although it is computationally more expensive than other unresolved-eddy turbulence models.[44,45] The exact transport equation for the transport of the Reynolds stress $\rho\overline{u'_i u'_j}$ in the RSM is written as[46]

$$\frac{\partial}{\partial t}(\rho\overline{u_i' u_j'}) + \frac{\partial}{\partial x_k}(\rho u_k \overline{u_i' u_j'}) = D_{T,ij} + P_{ij} + \varphi_{ij} + \varepsilon_{ij} \tag{4}$$

where ρ, u_i, u_i', and x_i are, respectively, liquid density, velocity, velocity fluctuation, and positional length. The two terms on the left are the local time derivative of the stress and convective transport term, respectively. The four terms on the right are the turbulent diffusion term $D_{T,ij}$, the stress production term P_{ij}, the pressure strain term ϕ_{ij}, and the dissipation term ε_{ij}. Their detailed description can be found in previous work.[41]

2.3. Mixture Model. The mixture model uses a single-fluid approach. The mixture model allows the phases to be interpenetrating. The volume fraction α_q for a control volume can therefore be equal to any value between 0 and 1, depending on the space occupied by the qth phase. The mixture model allows the phases to move at different velocities, using the concept of slip velocities. According to this model, the continuity equation for the mixture is[42]

$$\frac{\partial}{\partial t}(\rho_m) + \frac{\partial}{\partial x_i}(\rho_m u_m) = 0 \tag{5}$$

where u_m is the mass-averaged velocity:

$$u_m = \frac{\sum_{q=1}^{n} \alpha_q \rho_q u_q}{\rho_m} \tag{5a}$$

and ρ_m is the mixture density:

$$\rho_m = \sum_{q=1}^{n} \alpha_q \rho_q \tag{5b}$$

The momentum equation for the mixture can be obtained by summing the individual momentum equations for all phases. It can be expressed as

$$\frac{\partial}{\partial t}\rho_m u_{mi} + \frac{\partial}{\partial x_j}\rho_m u_{mi} u_{mj} = -\frac{\partial p}{\partial x_i} + \frac{\partial}{\partial x_j}\mu_m\left(\frac{\partial u_{mi}}{\partial x_j} + \frac{\partial u_{mj}}{\partial x_i}\right) + \rho g_i + \frac{\partial}{\partial x_j}\left(\sum_{q=1}^{n} \alpha_q \rho_q u_{dr,qi} u_{dr,qj}\right) \tag{6}$$

where n is the number of phases, and μ_m is the viscosity of the mixture:

$$\mu_m = \sum_{q=1}^{n} \alpha_q \mu_q \tag{6a}$$

where $u_{dr,q}$ is the drift velocity for secondary phase q, given by $u_{dr,q} = u_q - u_m$.

2.4. Stochastic Lagrangian Model for Coal Flow. The motion of a coal particle is described by the so-called stochastic Lagrangian multiphase flow model. The pressure gradient force and liquid drag force on particles are calculated in a Lagrangian reference frame. So the governing equation is written as

$$\frac{d\vec{u}_p}{dt} = F_D(\vec{u} - \vec{u}_p) + \frac{\vec{g}(\rho_p - \rho)}{\rho_p} + \left(\frac{\rho}{\rho_p}\right)\vec{u}_p\frac{\partial \vec{u}}{\partial x_i} \tag{7}$$

where $F_D(\vec{u} - \vec{u}_p)$ is the drag force per unit particle mass, given by

$$F_D = \frac{18\mu_m}{d_p^2 \rho_p} C_D \frac{Re_p}{24} \tag{8}$$

where $\vec{u}_p$ is the particle velocity, $\vec{u}$ is the velocity of the fluid phase, ρ_p is the density of the particle, and d_p is the particle diameter. Re_p is the relative Reynolds number, and C_D is the drag coefficient.

In the stochastic tracking approach, the turbulent dispersion of particles is predicted by integrating the trajectory equations for individual particles, using the instantaneous fluid velocity, $\bar{u} + u'$, along the particle path during the integration. The values of u' that prevail during the lifetime of the turbulent eddy are sampled by assuming that they obey a Gaussian probability distribution:

$$u' = \zeta\sqrt{\overline{u'^2}} \tag{9}$$

where ζ is a normally distributed random number. Because the kinetic energy k of turbulence is known at each point in the flow, the values of the root mean square fluctuating components can be obtained (assuming isotropy) as

$$\sqrt{\overline{u'^2}} = \sqrt{\overline{v'^2}} = \sqrt{\overline{w'^2}} = \sqrt{2k/3} \tag{10}$$

Particle−eddy interaction time and dimension should not be larger than the lifetime and size of a random eddy.

Note that the model described ignores the effect of coal particles on medium phase and the interaction between individual coal particles. This treatment has been widely accepted for dilute flows.[47,48] For dense flows, the so-called combined approach of CFD and discrete element method (CFD-DEM) can apply,[49−52] which is able to account for particle−particle and particle−fluid interactions. Such a CFD-DEM approach is also attempted in our DMC modeling as reported elsewhere.[53−55]

2.5. Calculation of "Medium" Viscosity. Medium viscosity is an important parameter describing the behavior of the medium flow and the separation of particles in DMCs. Its determination is complicated, because it depends on many variables, such as magnetite particle size distribution, particle shape, medium density, medium contamination, and so on.[56] In this work, viscosity is assumed to be controlled by the solid fraction of magnetite. Ishii and Mishima[57] proposed a model to describe the relationship between the medium viscosity and the solid fraction, given by

$$\frac{\mu_m}{\mu_c} = \left(1 - \frac{\alpha_d}{0.62}\right)^{-1.55} \tag{11}$$

where μ_m is the mixture viscosity, μ_c is the continuous phase (water) viscosity, and α_d is the solid volume fraction. However, this correlation is not general, and modification is necessary when applied to DMC modeling. In fact, as shown in Figure 2, eq 11 underestimates the medium viscosity measured by Napier-Munn and Scott.[17] A factor of 3.8 is found applicable to the magnetite system. It is noted that this method is empirical and only valid in a narrow range for equation formulation. So the following equation is used in the calculation of medium viscosity:

$$\mu_m = 3.8\mu_c\left(1 - \frac{\alpha_d}{0.62}\right)^{-1.55} \tag{12}$$

3. Simulation Conditions

Simulation conditions are similar to those used in the experimental studies by Subramanian[22] and Wood,[30] respectively. In this way, the validity of the preposed modeling can be examined by comparing the calculated and measured results. The geometrical parameters and operational conditions of the cyclones are listed in Table 1, where cases 1 and 2, respectively, correspond to the above two experimental studies.

Table 1. Geometry and Operational Conditions of the DMCs Considered

parameter	symbol	case 1	case 2
diameter of the body	D_c	350 mm	710 mm
side length of inlet	L_i	65 mm	132 mm
diameter of vortex finder	D_o	145 mm	294 mm
diameter of spigot	D_u	105 mm	248 mm
length of cylindrical part	L_c	200 mm	406 mm
length of vortex finder	L_v	127 mm	258 mm
length of conical part	L_p	695 mm	1410 mm
orientation angle		15°	10°
pressure at the two outlets (vortex finder and spigot)	P_{out}	101.325 kPa (open to atmosphere)	101.325 kPa (open to atmosphere)
inlet medium velocity	V_{in}	2.485 m/s	1.52 m/s
feed density	F_{rd}	1467 kg/m^3	1270 kg/m^3
magnetite sizes (and volume percentages)		2 (6%), 7 (10%), 15 (19%), 32 (38%), 54 (17%), and 82 μm (10%)	2 (4.9%), 7 (11.2%), 15 (24.1%), 32 (39.7%), 54 (12.4%), and 82 μm (7.7%)

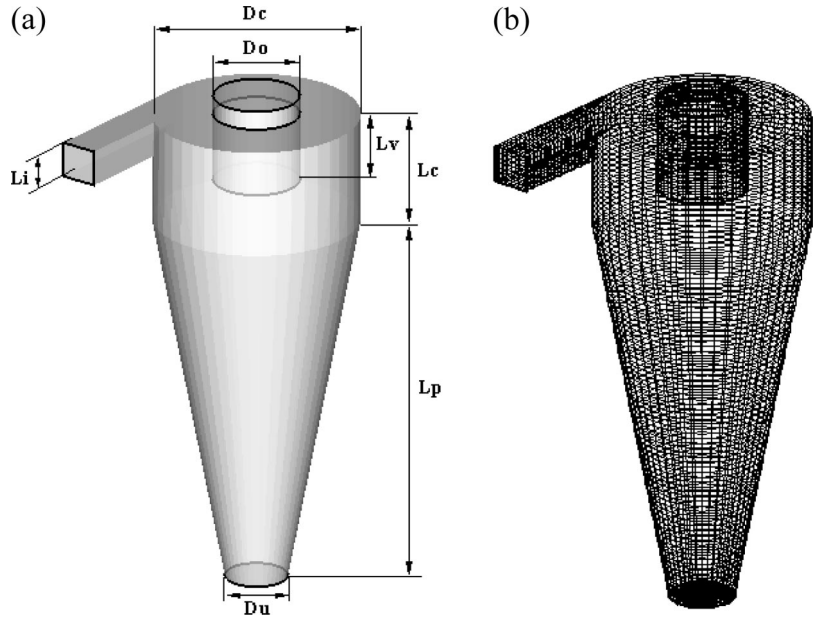

Figure 3. Schematic and grid representation of the DMC considered.

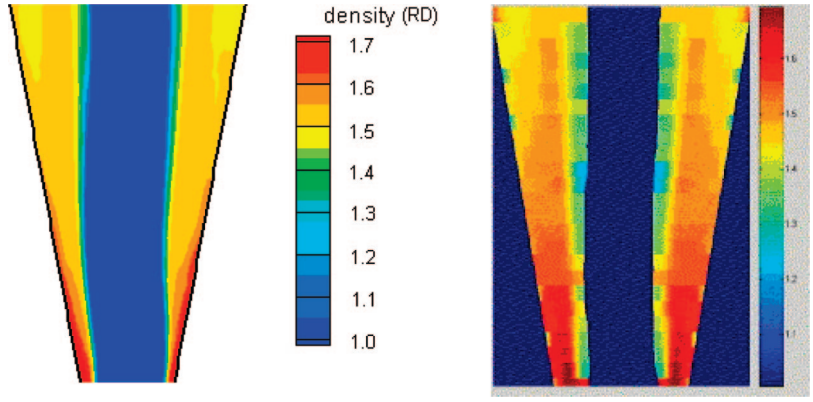

Figure 4. Comparison between the predicted (left) and measured (right) medium density distribution.

Figure 3a shows the notations of the DMC dimensions, and Figure 3b shows the computational domain. The whole computational domain is divided by 52 230 hexahedron grids. In the vicinity of the walls and vortex finder, the grid is more detailed than the remainder of the cyclone. Trial numerical results demonstrate that the solution is independent of the mesh size used.

Simulations are conducted using the Fluent CFD software package (v6.2). The second-order upwinding and the SIMPLE pressure−velocity coupling algorithm are used. The convergence strategy uses the unsteady solver, and the time step is chosen as $10^{-4}-10^{-2}$ s. Trial tests show that the results are not sensitive to the time step in this range for the considered DMC flows.

4. Results and Discussion

4.1. Model Validation. As described in section 2, the proposed modeling involves a few steps. This is because of the complexity of DMC flow and the absence of comprehensive experimental studies reported. The stepwise approach offers a way to use the existing data in verifying the proposed model.

The proposed model for step 1 is actually the same as that used in the modeling of the gas−liquid flow in a hydrocyclone. To validate this approach, the experimental data of Hsieh[7] were used. The predicted results are in good agreement with those measured, as reported elsewhere.[41]

Table 2. Comparison of the Predicted Flow Density with the Measured One and Available DMC Model Results[a]

data source	overflow density (kg/m^3)	underflow density (kg/m^3)
experimental values[22]	1375	2076
wood model[30]	1366	1868
Narasimha model[40]	1191	2055
the present model	1399	2032

[a] Feed density = 1467 kg/m^3.

Step 2 adds the medium, that is, magnetite particles, into consideration. In this work, six more phases, corresponding to the six magnetite size fractions, are considered, as listed in Table 1. To date, there are no data about the velocity profiles of such particle phases. What is available is the medium density distribution, measured by Subramanian.[22] Figure 4 shows the comparison of the measured and predicted density distributions (case 1). The profiles are very much similar. The model predictions of DMC efflux stream densities also compare very favorably with the measurements,[22] another CFD model used for the same situation,[40] and those predicted by a well-known empirical model,[30] as given in Table 2. Generally, the CFD models have a better prediction than the empirical Wood model.[30] The predicted overflow density of Narasimha model[40] is much lower than the measured one. The reason could be that the predicted velocity profile of the model in the inner flow

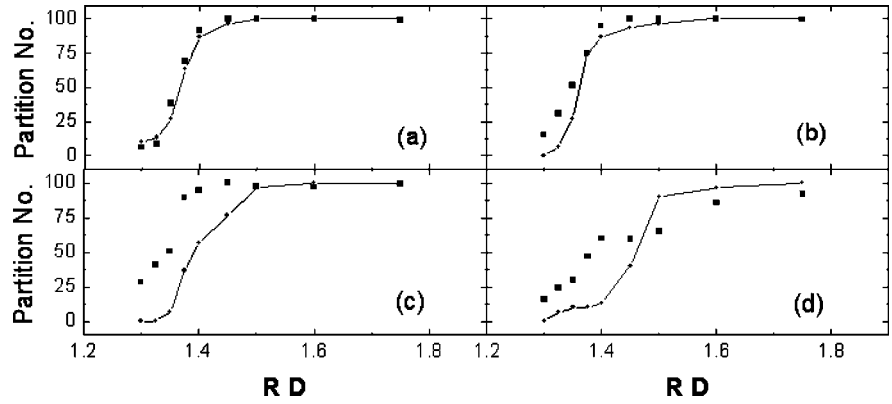

Figure 5. Comparison between the predicted and measured partition curves for coal particles with different size ranges: (a) 31.5 × 16 mm; (b) 16 × 8 mm; (c) 8 × 4 mm; (d) 2 × 1 mm; ■, measured; and −●−, predicted.

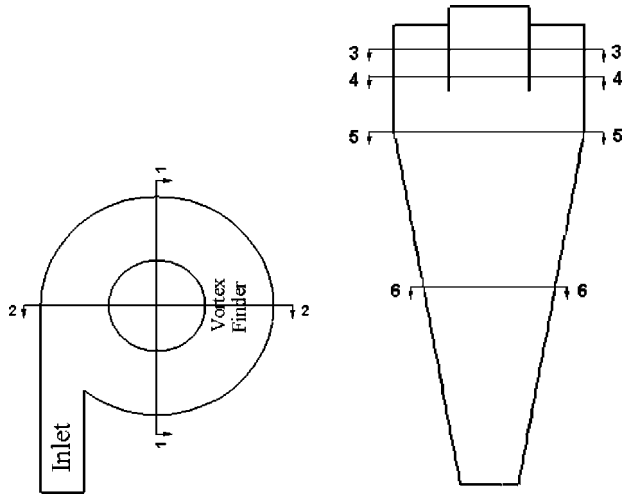

Figure 6. Definitions of the sections used in this work.

and air core does not follow the normal understanding in hydrocyclones.

Subramanian[22] did not provide the partition curve in his work, but such data are available in the work of Wood.[30] Therefore, the partition curve for different sized coal particles collected by Wood[30] is used to validate step 3 in the present modeling. Accordingly, the simulation conditions are changed (case 2 in Table 1). As shown in Figure 5, the predicted results appear to be in good agreement with those measured for coarse particles (larger than 8 mm), but poorer agreement is apparent for finer particles. Interestingly, it is also similar to the agreement found for a deterministic model in which tracer test results were extrapolated to the finer sizes.[26] The discrepancy is caused by many factors, for example, the different effect of viscous force on different sized particles, the neglect of some liquid−solid forces in the model, the noninteracting particle assumption inherent to the Lagrangian approach, and the experimental errors as well. The roles of these factors should be investigated in future studies. Despite the discrepancy observed, the results described above confirm that the model can generate information that can be used at least qualitatively in practice. In the following, we will use the model results to establish some general understanding about DMC flow and operations.

4.2. Medium Flow Pattern. To explore the inner flow in a DMC, different sections are used in the 350 mm DMC (case 1). Figure 6 shows the positions and identification numbers of six sections taken through the DMC. Section 1-1 is parallel to the inlet, and section 2-2 is perpendicular to the inlet. Sections 3-3, 4-4, 5-5, and 6-6 are located at the heights of 50, 100, 150, and 400 mm from the top wall situated on the roof of the cyclone. These sections are used in the figures in the following discussion.

Because a strong intensified vortex is formed in the cyclone body and a lot of fluid is thrown to the wall, the static pressure decreases rapidly from wall to center, as shown in Figure 7. The pressure gradient is the largest along the radial direction. So the pressure gradient force on a particle is high and dominant in the radial direction. The balance between the pressure gradient force and the centrifugal force, which corresponds to the swirling flow, determines the destination of coal particles. When the pressure gradient force on a coal particle is larger than the centrifugal force, the particle reports to the overflow and is carried out of the cyclone through the vortex finder; otherwise, it is discharged through the spigot. Therefore, the pressure gradient force is very important for the DMC operation, although it is not considered in many other particle−fluid flows, for example, gas fluidization[51] and gas cyclone.[58]

Figure 8 shows the calculated tangential velocity distribution in detail. The flow field in the DMC indicates the expected forced/free combination of the Rankine vortex.[59] The value of the tangential velocity is zero at the wall and at the center of the flow field (air core is a forced vortex). From section 3-3, it can be seen that the flow enters the inlet and accelerates up to 1.5−2.0 times of that at the inlet (point A). The velocity then decreases as the flow spins down along the wall. Before it passes below the vortex finder, the fluid flow collides with the follow-up flow and forms a chaotic flow close to the vortex finder outside wall (point B). Because of the collision, part of the fluid flows down along the outside wall of the vortex finder. Once this flow reaches the bottom of the vortex finder, it turns and escapes rapidly from the overflow. As well as creating a bypass opportunity, this behavior called the short circuit flow would increase the loss of energy and separation efficiency in the DMC.

Figure 9 shows the calculated axial velocity distribution. The black line in the figure represents the dividing line between the upward flow and the downward flow, known as the locus of zero vertical velocity.[4] The upward flow in the DMC is a helical twisted cylinder and not axially symmetric, especially in the conical section. The diameter of upward flow is larger than that of the vortex finder. Moreover, because the upward flow swarms into the vortex finder and the short circuit flow goes out from the vortex finder, the axial velocity reaches a peak value under the vortex finder. A proportion of the feed medium passes directly across the cyclone roof and down the outside wall of the vortex finder to join the overflow stream within the vortex finder, and represents a short circuit flow (point A). At point B, a vertical flow can exist in the region between the outer wall

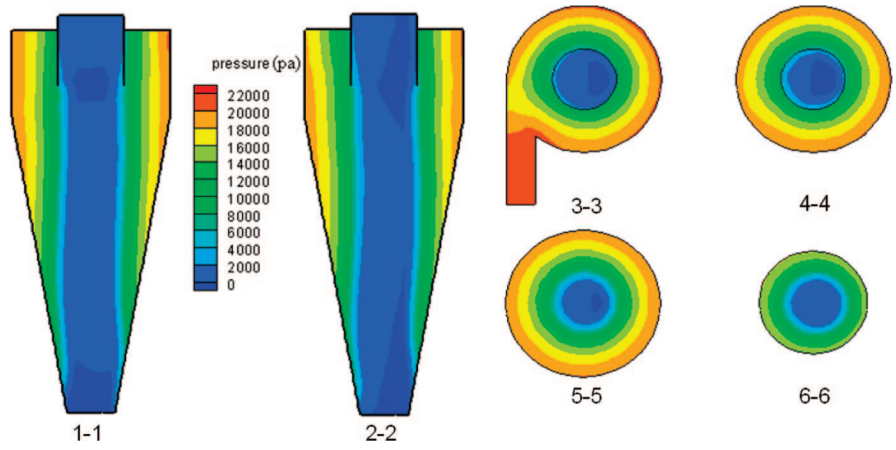

Figure 7. Distribution of pressure in the DMC.

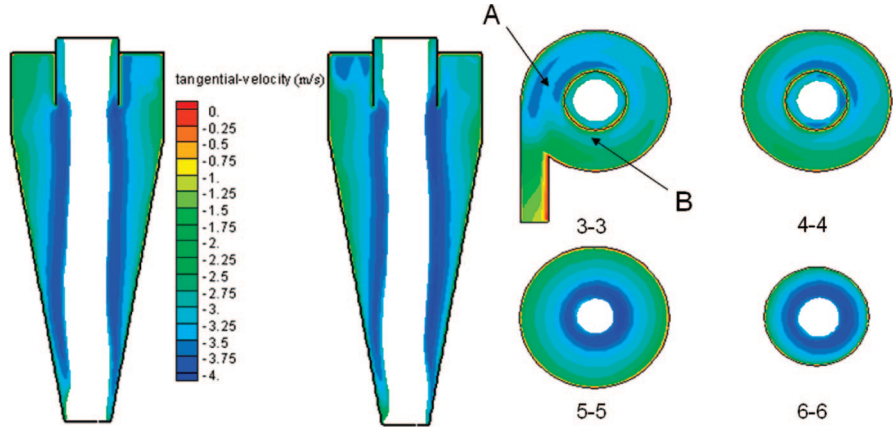

Figure 8. Distribution of tangential velocity in the DMC (anticlockwise is positive and clockwise is negative).

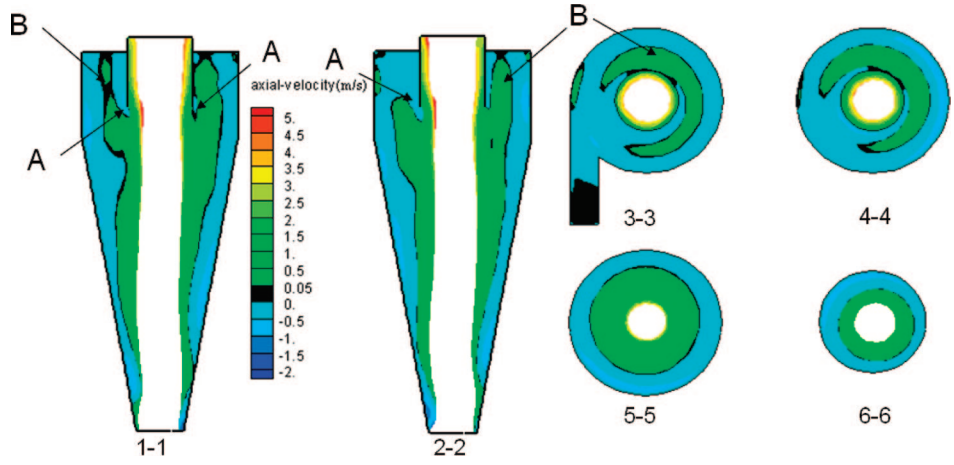

Figure 9. Distribution of axial velocity in the DMC (upward is positive and downward is negative, and the black line is the division between the upward and downward flows).

of vortex finder and the wall of body. This is known as the eddy flow[4] and is characterized by recirculating currents.

Figure 10 shows the calculated radial velocity distribution. The distribution is like a helical twisted cylinder. The axis of the forced vortex does not coincide with the geometrical axis of the DMC and is curved rather than straight. The distribution of radial velocity in the central core vortex is eccentric with respect to the central axial line. The value of one side is positive, and the other is negative. So, the combination of flow source and sink is distributed near the axis of the cyclone, forming a pattern of flow dipoles. The orientation of a dipole is located upward along the cyclone central line. The main reason for this phenomenon is the internal flow collisions, which may cause instability in the DMC. There is a zone under the vortex finder, at point A (sections 1-1 and 2-2), where fluid directly flows into the vortex finder rather than moving down to the conical part and then flowing upward. Moreover, at point B (section 3-3), the radial velocity becomes negative again and directs the flow to the center because of the collision of the fluid streams. These result in a short circuit flow, which reduces the DMC performance.

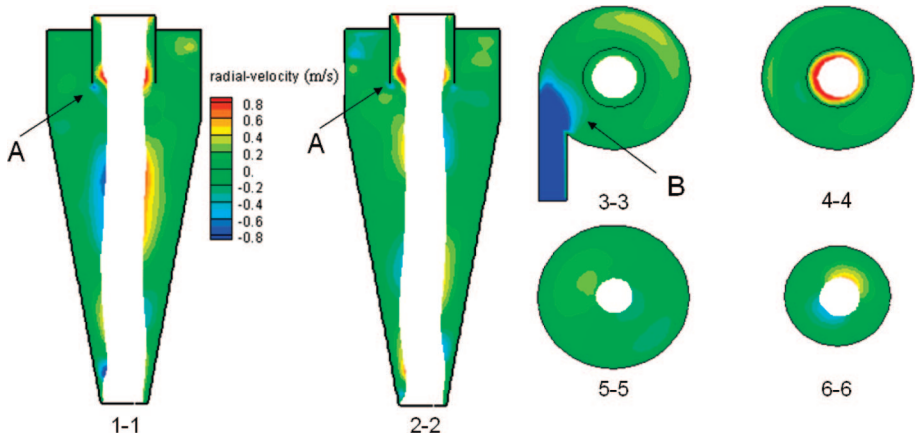

Figure 10. Distribution of radial velocity in the DMC (outward is positive and inward is negative).

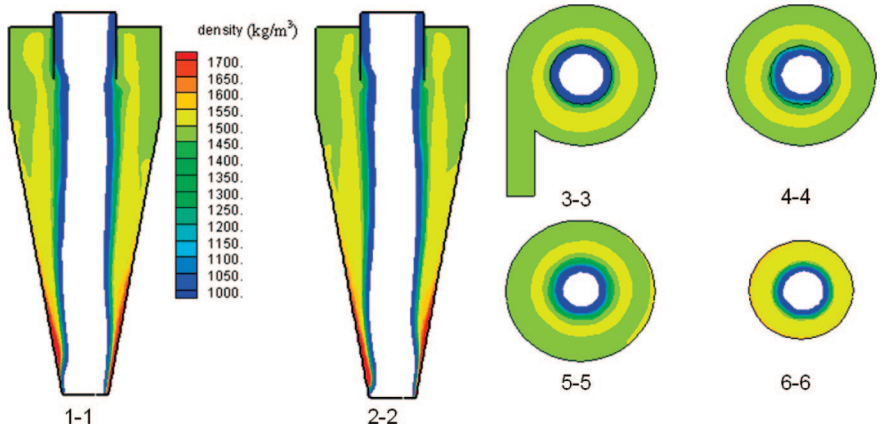

Figure 11. Distribution of density in the DMC.

Figure 11 presents the density distribution in the DMC. Generally, the density at the lower part is higher than that at the upper part, and the density distribution decreases radially from wall to center. The peak value occurs at the bottom of the DMC, near the spigot. Moreover, a high density ring exists around the air core with a diameter larger than that of the vortex finder.

The predicted distributions of magnetite particles of various sizes inside the cyclone are shown in Figure 12. The legend beside the figure shows the ratio of the volume fraction of each size particle in the cyclone to that in the feed. As expected, the ultrafine particles such as 2, 7, and 15 μm are distributed quite uniformly. The 32 and 54 μm magnetite particles accumulate on the wall near the spigot and have a high density ring around the air core due to the upward flow. Most 82 μm magnetite particles segregate toward the wall and develop a high concentration near the spigot. The segregation near the spigot in the medium occurs on the respective coarse magnetite particles, such as 32, 54, and 82 μm in this case. When the segregation is intensive, the density differential would be high, which is defined as the difference between the underflow and overflow density. In this situation, some heavy particles could be pushed to the upward flow and report to the overflow, resulting in a bad separation performance.

4.3. Particle Flow Pattern. Five typical coal particles (the diameter of particles is 5 mm) of different densities were chosen to track their trajectories in the DMC. As shown in Figure 13, heavy particles (RD = 1.6 and 1.7) are rejected through the spigot, while light particles (RD = 1.2, 1.3, and 1.4) escape from the vortex finder. Particles with small density cannot move outward to the cyclone wall because the centrifugal force acting on them is insufficient to overcome the fluid drag force and pressure gradient force. An approximate cut point particle (RD = 1.5) is initially dragged down by the external downward flow. At the same time, the pressure gradient force toward the air core causes particles to be dragged inward. Consequently, in some part of the conical section, such a particle is caught by the upward inner flow and escapes through the vortex finder, or follows the external downward flow to be collected at the underflow. The cut point particle is unstable and has a larger residence time than do other particles of different densities.

Figure 14 shows the spatial distribution of particles of different densities in the DMC, in which the diameter of coal particles is 5 mm. It can be seen that the distribution of coal particles of different densities in the DMC is stratified along the axial direction. First, there are no particles in the air core. The ultralight particles (1.2 RD, blue) only appear at the cylindrical part in the DMC and escape from the vortex finder. As RD increases, the range of particle dispersions (1.3 and 1.4 RD, green and yellow) extends to the conical section. Particles at 1.5 RD (orange) can discharge from both overflow and underflow and are distributed quite uniformly, except for a concentration around the air core. The heavy particles (1.6 RD, red) are concentrated at the wall and escaped from the underflow. Furthermore, particles leave the wall and float on the medium at the end of the conical part, where the density of the medium is higher than that of particles (RD = 1.6), as shown in the medium density distribution (Figure 11). The reason is that the segregation of magnetite particles is serious in this area, as described in Figure 12.

Figure 15 shows the calculated separation efficiency as a function of coal particle density. Each point in a partition curve

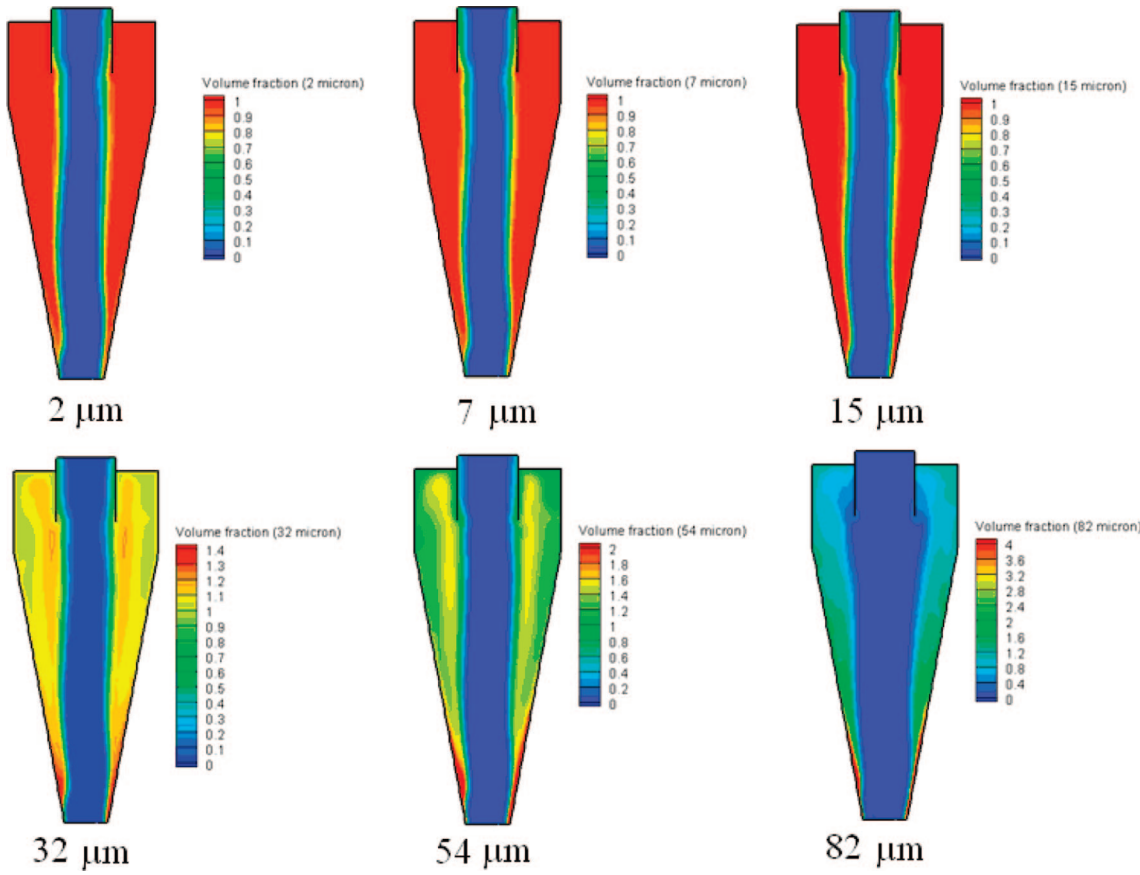

Figure 12. Distribution of magnetite particles of different sizes in the DMC.

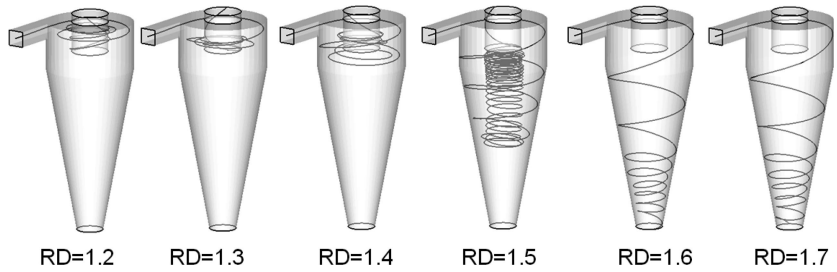

Figure 13. Typical trajectories of coal particles with different densities when the medium feed relative density is 1.467.

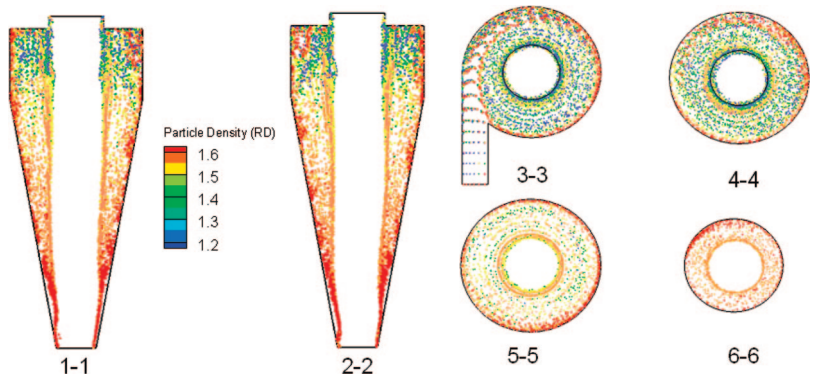

Figure 14. The distribution of coal particles of different densities in the DMC.

is obtained by tracking 15 000 particles to be statistically representative. Furthermore, the inset in the figure shows the partition coefficient, that is, the weight percent reported to underflow, as a function of size for particles whose density is 1.54 RD. It can be seen that the partition coefficient increases with decreasing particle size beyond a critical particle size. This is known as the "fish-hook" effect in hydrocyclones.[60−63] The results in Figure 15 indicate this phenomenon can also be found in DMCs.

The separation performance of particles depends on their sizes and densities. The so-called cut point RD_{50} (the particle density at which the DMC separation efficiency is 50%) and Ecart

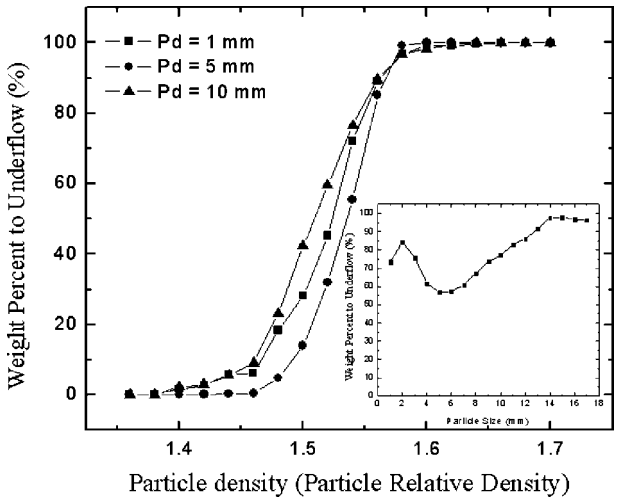

Figure 15. The partition curve of the DMC.

probable E_p (=(RD_{75} − RD_{25})/2) are the two parameters commonly used to assess separation efficiency in industry and can be obtained from the partition curve. For example, for 5 mm coal particles, RD_{50} equals 1.54 RD, and E_p is approximately 0.025 from Figure 15. When expressed as a function of particle size, Figure 16 presents the general performance for DMC separation in terms of the cut point and E_p. The trend of numerical results agrees reasonably well with that observed in experiments or in industry.[30] Interestingly, a "breakaway size" where efficiency sharply deteriorates is also identified to be the same as that found experimentally,[30] which is around 1 mm for this DMC.

4.4. Flow Instability in DMCs. The flow field in a DMC is unsteady in a separation operation. The flow rates of underflow and overflow fluctuate limitedly in a normal operation. All of the above results are generated under such macroscopically stable conditions. However, if a DMC is not properly designed or in poor operational conditions, the fluctuation will become more serious, resulting in the so-called "surging". Surging is a complex phenomenon that is difficult to predict. It was considered to be related to the instability of particle flow when the ratio of medium-to-coal is too low in the recent CFD-DEM work.[55] In this work, it is found that the instability of medium flow could cause the surging too, particular when the DMC was not properly designed. As an example, an altered DMC geometry is used, done by reducing the length of the conical part (L_p).

Figure 17 shows the air core diameters for simulations with and without surging. The black line in the figure indicates the

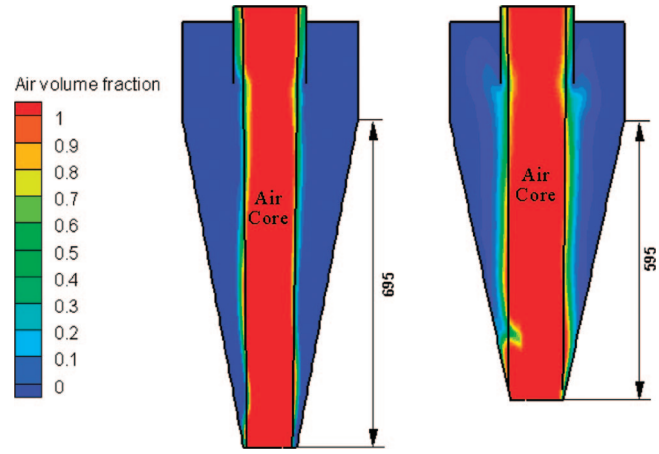

Figure 17. The shape of the air core in the DMCs under normal (left) or surging (right) operation.

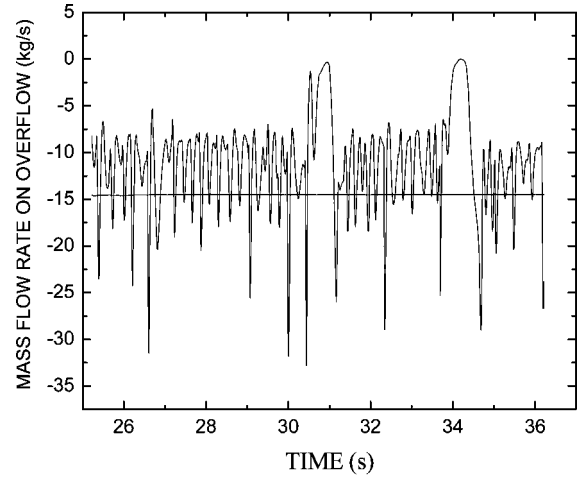

Figure 18. The change of mass flow rate on the overflow (straight, horizontal line, normal; fluctuated line, surging).

boundary of the air core. The left diagram presents a standard DMC design with 695 mm conical section. The diameter of air core is less than that of the spigot and the flow field remains macroscopically stable, and surging does not occur. The right diagram presents the air volume fraction in the DMC with 595 mm conical part. It indicates that the air core diameter increases to that of the spigot. In such a DMC, the fluid should flow down along the wall and exit through spigot. However, the spigot is filled with fast flowing air. Therefore, when the diameter of the air core reached that of the spigot, the fluctuation of the flow

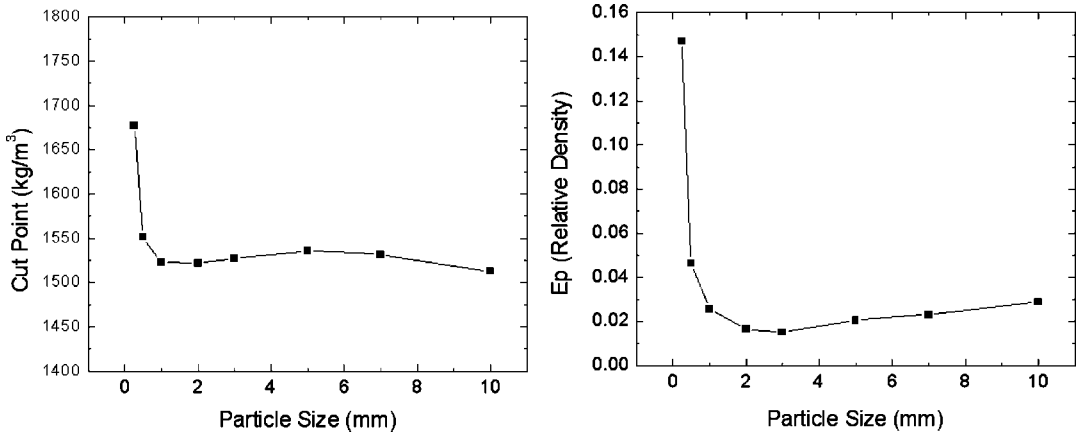

Figure 16. Separation performance in terms of cut point (left) and E_p (right) versus particle size.

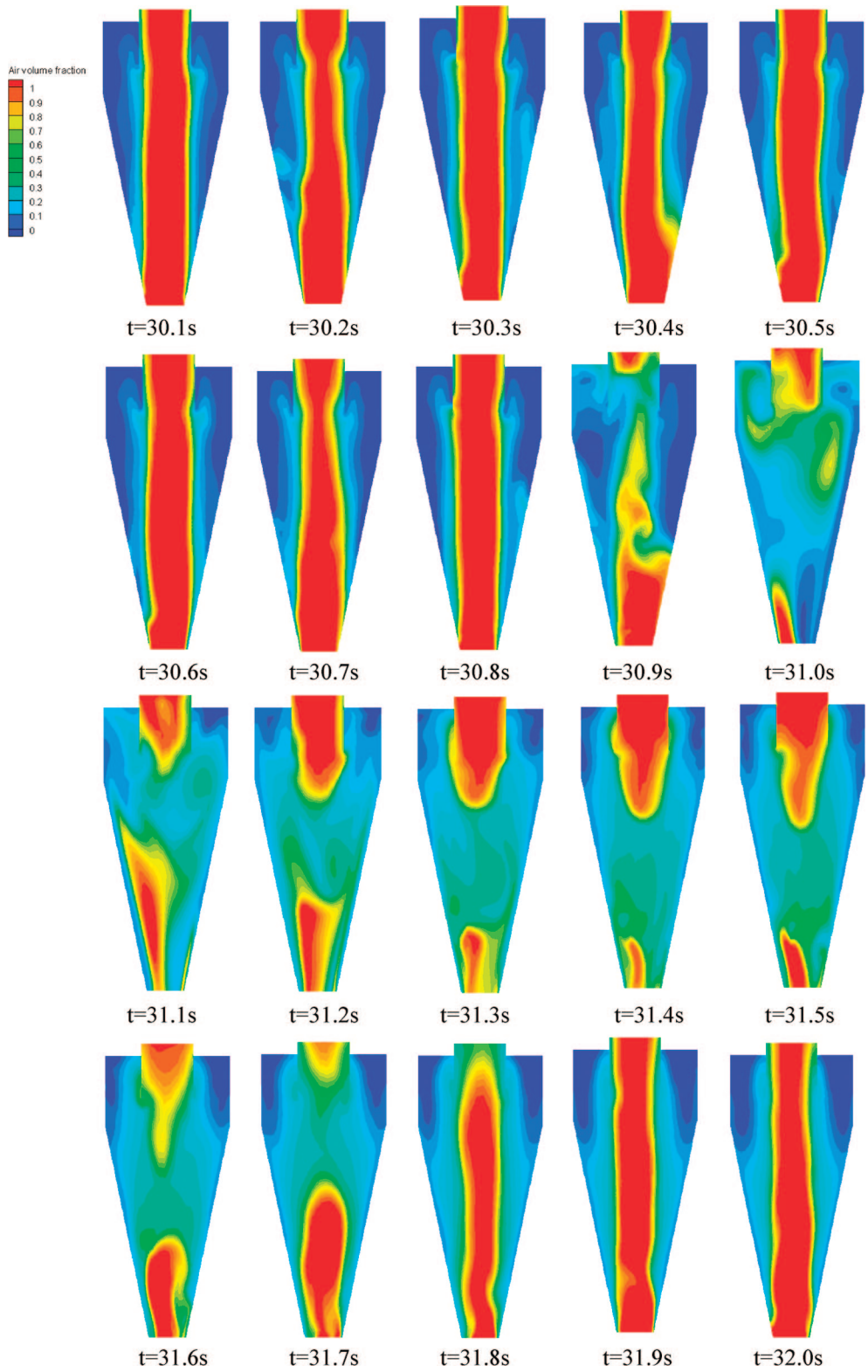

Figure 19. Snapshots showing the surging phenomenon in the DMC.

rates at both overflow and underflow became very significant, and the interaction between fluid and air became quite intense and caused flow instability in the DMC.

Figure 18 shows the variation in overflow flow rate when the process is normal (straight line) and surging occurs (fluctuated line). In normal operation, the overflow flow rate is approximately 14.5 kg/s with a negligible fluctuation. When surging occurs, the fluctuation becomes significant and the air core becomes unstable, which indicate that surging caused the overflow rate to vary between 7 and 17 kg/s. Corresponding to this fluctuation, the air core can be destroyed and reformed, as discussed below.

Figure 19 shows the evolution of air volume fraction in the cyclone with time. The results demonstrate how the surging in the DMC is developed. At the beginning stage (30.1−30.8 s), air core is still there but becomes unstable. The medium can report to the underflow through only one side of the spigot because of the strong air core. At the same time, some medium

accumulates in the DMC. Under this condition, the medium reporting to the underflow would be very low. In other words, the medium differential (defined as the difference in the RD between the overflow and underflow) is very high, consistent with the experimental observation.[30] In the next stage (30.9−31.4 s), more and more medium accumulates in the conical part, and at last the accumulated medium breaks down the air core and flows rapidly to the underflow. The air core in the lower part disappears, and only its upper part in the vortex finder remains. Note that the air in the upper part comes from overflow remaining cone-shaped in the vortex.[41] Next (at 31.4−32 s), the air core is rebuilt for the underflow. Such instable flow can be observed periodically or irregularly as shown in Figure 18 (33−35 s). In a surging period, shale and raw coal would reject from the underflow, resulting in a bad separation performance. It is important to design and control DMCs properly to avoid surging.

5. Conclusions

A CFD model has been developed to describe the multiphase flow in a DMC. Its applicability is demonstrated by the good agreement between the calculated and measured results under different conditions reported in the literature. The model offers a convenient method to study the flow and performance of DMCs.

The computed results confirm that the flow field in a DMC is similar to that in a hydrocyclone. Thus, it is observed that there is collision between fluid streams after running about a circle with that just entering in a DMC leading to a short circuit flow. The combination of flow source and sink distributes near the axis of cyclone, forming a pattern of flow dipole. The orientation of dipole is observed to locate upward along the cyclone central line. Also, the forced vortex in the cyclone is a twisted cylinder.

However, the flow field in a DMC is much more complicated, featured with some particular characteristics not observed in a hydrocyclone. For example, a high density ring with a diameter larger than the vortex finder is present around the air core. The segregation near the spigot in the medium occurs for coarse magnetite particles. The distribution of coal particles of different densities in a DMC is stratified along the axial direction. Notably, the so-called "fish hook" phenomenon can also be found for coal particles. The instability of medium flow, which may result from improper DMC design or operation, can cause surging. There is a need for more intensive studies to understand the flow phenomena under different DMC conditions.

Acknowledgment

We are grateful to the Australian Coal Association Research Program (ACARP) and Australia Research Council (ARC) for the financial support of this work, and the industrial monitors, Harvey Crowden, Dion Lucke, Ian Brake, and Peter Newling, for helpful discussion and suggestions.

Nomenclature

C_D = drag coefficient
d = particle diameter, m
$D_{T,ij}$ = turbulent diffusion term
F_D = defined by eq 11
g = acceleration due to gravity, m s^{-2}
k = kinetic energy, m^2 s^{-2}
p = static pressure, Pa
P_{ij} = stress production term
Re = Reynolds number
t = time, s
u = instantaneous velocity, m s^{-1}
v = instantaneous velocity, m s^{-1}
w = instantaneous velocity, m s^{-1}
u' = dispersion velocity, m s^{-1}
$\bar{u}$ = time average velocity in axial direction, m s^{-1}
x = axis, m
α = volume fraction
ε_{ij} = dissipation term
ϕ_{ij} = pressure strain term
μ = fluid viscosity, kg m^{-1} s^{-1}
ρ = density, kg m^{-3}
ζ = normally distributed random number

Subscripts

c = continuous phase
d = solid phase
dr = drift velocity
i, j, k = 1, 2, 3
m = mixture
p = particle
q = qth phase

Literature Cited

(1) Wills, B. A.; Napier-Munn, T. J. *Wills' Mineral Processing Technology*, 7th ed.; Butterworth-Heinemann: Oxford, UK, 2006.

(2) Svarovsky, L. *Hydrocyclones*; Technomic Publishing Inc.: Lancaster, PA, 1984.

(3) King, R. P.; Juckes, A. H. Cleaning of fine coals by dense-medium hydrocyclone. *Powder Technol.* **1984**, *40*, 147–160.

(4) Bradley, D. *The Hydrocyclone*; Pergamon: London, 1965.

(5) Concha, F.; Barrientos, A.; Montero, J.; Sampaio, R. Air core and roping in hydrocyclones. *Int. J. Miner. Process.* **1996**, *44−5*, 743–749.

(6) Dai, G. Q.; Chen, W. M.; Li, J. M.; Chu, L. Y. Experimental study of solid-liquid two-phase flow in a hydrocyclone. *Chem. Eng. J.* **1999**, *74*, 211–216.

(7) Hsieh, K. T. Phenomenological model of the hydrocyclone. Ph.D. Thesis, The University of Utah, 1988.

(8) Hsieh, K. T.; Rajamani, R. K. Mathematical-model of the hydrocyclone based on physics of fluid flow. *AIChE J.* **1991**, *37*, 735–746.

(9) Knowles, S. R.; Woods, D. R.; Feuerste, I. Velocity distribution within a hydrocyclone operating without an air core. *Can. J. Chem. Eng.* **1973**, *51*, 263–271.

(10) Monredon, T. C.; Hsieh, K. T.; Rajamani, R. K. Fluid-flow model of the hydrocyclone - an investigation of device dimensions. *Int. J. Miner. Process.* **1992**, *35*, 65–83.

(11) Rietema, K.; Verver, C. G. *Cyclones in Industry*; Elsevier: Amsterdam, 1961.

(12) Dunglison, M. E.; Napier-Munn, T. J. Measuring flow rate in the dense medium cyclone. *Trans. Inst. Min. Metall., Sect. C* **2002**, *111*, C163–C165.

(13) Ferrara, G.; Bevilacqua, P.; De Lorenzi, L.; Zanin, M. The influence of particle shape on the dynamic dense medium separation of plastics. *Int. J. Miner. Process.* **2000**, *59*, 225–235.

(14) Fourie, P. J. F.; Vanderwalt, P. J.; Falcon, L. M. The beneficiation of fine coal by dense-medium cyclone. *J. South Afr. Inst. Min. Metall.* **1980**, *80*, 357–361.

(15) He, Y. B.; Laskowski, J. S. Effect of dense medium properties on the separation performance of a dense medium cyclone. *Miner. Eng.* **1994**, *7*, 209–221.

(16) Klima, M. S.; Kim, B. H. Dense-medium separation of heavy-metal particles from soil using a wide-angle hydrocyclone. *J. Environ. Sci. Health, Part A* **1998**, *33*, 1325–1340.

(17) Napier-munn, T. J.; Scott, I. A. The effect of demagnetization and ore contamination on the viscosity of the medium in a dense medium cyclone plant. *Miner. Eng.* **1990**, *3*, 607–613.

(18) Restarick, C. J.; Krnic, Z. The effect of underflow overflow ratio on dense medium cyclone operation. *Miner. Eng.* **1991**, *4*, 263–270.

(19) Svoboda, J.; Coetzee, C.; Campbell, Q. P. Experimental investigation into the application of a magnetic cyclone for dense medium separation. *Miner. Eng.* **1998**, *11*, 501–509.

(20) Turek, M. L.; Klima, M. S. Dense-medium cycloning of fine coal refuse material. *Coal Prep.* **2003**, *23*, 267–284.

(21) Galvin, K. P.; Smitham, J. B. Use of X-rays to determine the distribution of particles in an operating cyclone. *Miner. Eng.* **1994**, *7*, 1269–1280.

(22) Subramanian, V. J. Measurement of medium segregation in the dense medium cyclone using gamma-ray tomography. Ph.D Thesis, University of Queensland, 2002.

(23) Barbee, C. J.; Luttrell, G. H.; Wood, C. J.; Bethell, P. J. Simulation of heavy medium cyclone performance. *Miner. Metall. Process.* **2005**, *22*, 38–42.

(24) Davis, J. J. A study of coal washing dense medium cyclones. Ph.D. Thesis, University of Queensland, 1987.

(25) Honaker, R. Q.; Singh, N.; Govindarajan, B. Application of dense-medium in an enhanced gravity separator for fine coal cleaning. *Miner. Eng.* **2000**, *13*, 415–427.

(26) Hu, S.; Firth, B.; Vince, A.; Lees, G. Prediction of dense medium cyclone performance from large size density tracer test. *Miner. Eng.* **2001**, *14*, 741–751.

(27) Napier-munn, T. J. Modeling and simulating dense medium separation processes - a progress report. *Miner. Eng.* **1991**, *4*, 329–346.

(28) Sripriya, R.; Banerjee, P. K.; Rao, P. V. T.; Dutta, A.; Rao, M. V. S. Critical evaluation of factors affecting the operation of dense medium cyclones treating medium coking coals. *Int. J. Miner. Process.* **2001**, *63*, 191–206.

(29) Sripriya, R.; Rao, P. V. T.; Bapat, J. P.; Singh, N. P.; Das, P. Development of an alternative to magnetite for use as heavy media in coal washeries. *Int. J. Miner. Process.* **2003**, *71*, 55–71.

(30) Wood, J. C. A performance model for coal-washing dense medium cyclones. Ph.D. Thesis, University of Queensland, 1990.

(31) Zughbi, H. D.; Schwarz, M. P.; Turner, W. J.; Hutton, W. Numerical and experimental investigations of wear in heavy medium cyclones. *Miner. Eng.* **1991**, *4*, 245–262.

(32) Clarkson, C. J.; Edward, D. J.; Davidson, J.; Lahey, A. E. Analysis of large diameter cyclone plant data. In *The 9th Australian Coal Preparation Conference*; Firth, B., Ed.; Yeppoon, Australia, 2002.

(33) Weale, W.; Swanson, A. Improved design and operational data for large diameter dense medium cyclones. In *The 9th Australian Coal Preparation Conference*; Firth, B., Ed.; Yeppoon, Australia, 2002.

(34) Gay, S. Mathematical methods for estimating washability curves. Australian Coal Association Research Program (ACARP), Project C7045, 1999.

(35) Rong, R. Feasibility study of a new cyclone design concept for fine coal and optimisation of the new classification cyclone design. Australian Coal Association Research Program (ACARP), Projects C7043 and C8048, 2000.

(36) Rong, R. New dense medium cyclone design. Australian Coal Association Research Program (ACARP), Project C9044, 2001.

(37) Weale, W.; Swanson, A. Large diameter dense medium cyclone operation data. Australian Coal Association Research Program (ACARP), Project C10048, 2002.

(38) Suasnabar, D. J.; Fletcher, C. A. J. A CFD model for dense medium cyclones. *Second International Conference on CFD in the Minerals and Process Industries*; CSIRO, Melbourne, Australia, 1999.

(39) Brennan, M. S. Multiphase CFD simulations of dense medium and classifying hydrocyclones. *Third International Conference on CFD in the Minerals and Process Industries*; CSIRO, Melbourne, Australia, 2003.

(40) Narasimha, M.; Brennan, M. S.; Holtham, P. N. Numerical simulation of magnetite segregation in a dense medium cyclone. *Miner. Eng.* **2006**, *19*, 1034–1047.

(41) Wang, B.; Chu, K. W.; Yu, A. B. Numerical study of particle-fluid flow in a hydrocyclone. *Ind. Eng. Chem. Res.* **2007**, *46*, 4695–4705.

(42) Manninen, M.; Taivassalo, V.; Kallio, S. *On the Mixture Model for Multiphase Flow*; VTT Publications: Finland, 1996.

(43) Batchelor, G. K. *An Introduction to Fluid Dynamics*; Cambridge Univ. Press: Cambridge, England, 1967.

(44) Hoekstra, A. J.; Derksen, J. J.; Van Den Akker, H. E. A. An experimental and numerical study of turbulent swirling flow in gas cyclones. *Chem. Eng. Sci.* **1999**, *54*, 2055–2065.

(45) Sommerfeld, M.; Ho, C. A. Numerical calculation of particle transport in turbulent wall bounded flows. *Powder Technol.* **2003**, *131*, 1–6.

(46) Launder, B. E.; Reece, G. J.; Rodi, W. Progress in development of a Reynolds-stress turbulence closure. *J. Fluid Mech.* **1975**, *68*, 537–566.

(47) Ma, L.; Ingham, D. B.; Wen, X. Numerical modelling of the fluid and particle penetration through small sampling cyclones. *J. Aerosol Sci.* **2000**, *31*, 1097–1119.

(48) Narasimha, M.; Brennan, M.; Holtham, P. N. Large eddy simulation of hydrocyclone--prediction of air-core diameter and shape. *Int. J. Miner. Process.* **2006**, *80*, 1–14.

(49) Chu, K. W.; Yu, A. B. Numerical simulation of complex particle-fluid flows. *Powder Technol.* **2008**, *179*, 104–114.

(50) Feng, Y. Q.; Yu, A. B. Assessment of model formulations in the discrete particle simulation of gas-solid flow. *Ind. Eng. Chem. Res.* **2004**, *43*, 8378–8390.

(51) Xu, B. H.; Yu, A. B. Numerical simulation of the gas-solid flow in a fluidized bed by combining discrete particle method with computational fluid dynamics. *Chem. Eng. Sci.* **1997**, *52*, 2785–2809.

(52) Yu, A. B.; Xu, B. H. Particle-scale modelling of gas-solid flow in fluidisation. *J. Chem. Technol. Biotechnol.* **2003**, *78*, 111–121.

(53) Chu, K. W.; Wang, B.; Yu, A. B.; Vince, A. Modelling the coal-medium flow in a dense medium cyclone. *The 12th Australian Coal Preparation Conference and Exhibition*; Sydney, Australia, 2008.

(54) Wang, B.; Chu, K. W.; Yu, A. B.; Vince, A. Estimation of steady state and dynamic dense medium cyclone performance. Australian Coal Association Research Program (ACARP), C15052, 2007.

(55) Chu, K. W.; Wang, B.; Yu, A. B.; Vince, A. CFD-DEM modelling of the multiphase flow in dense medium cyclone. *Powder Technol.*, in press.

(56) He, Y. B.; Laskowski, J. S.; Klein, B. Particle movement in non-Newtonian slurries: the effect of yield stress on dense medium separation. *Chem. Eng. Sci.* **2001**, *56*, 2991–2998.

(57) Ishii, M.; Mishima, K. Two-fluid model and hydrodynamic constitutive relations. *Nucl. Eng. Des.* **1984**, *82*, 107–126.

(58) Wang, B.; Xu, D. L.; Chu, K. W.; Yu, A. B. Numerical study of gas-solid flow in a cyclone separator. *Appl. Math. Modell.* **2006**, *30*, 1326–1342.

(59) Panton, R. L. *Incompressible Flow*, 2nd ed.; John Wiley & Sons: New York, 1996.

(60) Dueck, J. G.; Min'kov, L. L.; Pikushchak, E. V. Modeling of the "fish-hook" effect in a classifier. *J. Eng. Phys. Thermophys.* **2007**, *80*, 64–73.

(61) Kraipech, W.; Chen, W.; Parma, F. J.; Dyakowski, T. Modelling the fish-hook effect of the flow within hydrocyclones. *Int. J. Miner. Process.* **2002**, *66*, 49–65.

(62) Majumder, A. K.; Yerriswamy, P.; Barnwal, J. P. The "fish-hook" phenomenon in centrifugal separation of fine particles. *Miner. Eng.* **2003**, *16*, 1005–1007.

(63) Roldan-Villasana, E. J.; Williams, R. A.; Dyakowski, T. The origin of the fish-hook effect in hydrocyclone separators. *Powder Technol.* **1993**, *77*, 243–250.

Received for review July 31, 2008
Revised manuscript received January 12, 2009
Accepted January 20, 2009

IE801175C